INTEGRATED DESIGN OF SUPERCONDUCTING ACCELERATOR MAGNETS

S. Russenschuck, C. Paul, S. Ramberger, F. Rodriguez-Mateos, R. Wolf
CERN, 1211 Geneva 23, Switzerland

Abstract
This chapter introduces the main features of the ROXIE program which has been developed for the design of the superconducting magnets for the Large Hadron Collider (LHC) at CERN. The program combines numerical field calculation with a reduced vector-potential formulation, the application of vector-optimization methods, and the use of genetic as well as deterministic minimization algorithms. Together with the applied concept of features, the software is used as an approach towards integrated design of superconducting magnets. The main quadrupole magnet for the LHC, was chosen as an example for the integrated design process.

1 Introduction

The Large Hadron Collider (LHC) project is a superconducting accelerator for protons, heavy ions and electron- proton collisions in the multi-TeV energy range to be installed at CERN [1]. In order to achieve the design energy within the constraint of the existing LEP tunnel, which has a circumference of about 27 km, the magnet system must operate in superfluid helium below 2 K. The tunnel's limited space, as well as cost considerations, dictate a two-in-one magnet design, where the two rings are incorporated into the same cryostat. The main dipole magnets will operate at about 0.54 T at injection and 8.40 T at nominal current. The main quadrupoles, will operate at a 223 T/m field gradient, a magnetic length of 3.10 m, a nominal current of 11800 A, an inner coil aperture of 50 mm, and an operational temperature of 1.8 K. For the optimization of the magnets, contradictory parameters such as maximum main field, minimum content of unwanted multipoles, and sufficient safety margin for the conductor must be considered. The keystoning of the conductors and the resulting grading of the current densities necessitate a computational method that can model the coil and calculate the excitational field with a higher accuracy than rendered by most of the commercial finite element packages. In addition, the characteristic data for both the coil and the iron configuration must be parametric for the application of mathematical optimization techniques.

Together with the module for the addressing input and output data as design variables or design objectives, the Feature-Based Design Module (FBDM) can be seen as the heart of the ROXIE program. This program has been developed at CERN for the design and optimization of the coil and yoke geometries for the superconducting magnets for the Large-Hadron-Collider, LHC. Features are functional primitives that contain not only the geometrical information (shape, dimensions, position, orientation, tolerances) of a part, but also non-geometric properties such as material name, properties, part number, etc. Designing by features is therefore an extension to parametric programming and is used together with mathematical optimization techniques and numerical field calculation as an approach towards an integrated design of superconducting magnets [5]. The steps in the design process are:

- Feature-based geometry creation.
- Conceptual design using genetic algorithms.

- Calculation of field errors caused by persistent currents.
- Optimization of the coil cross-section.
- Minimization of iron-induced multipoles.
- Quench simulation.
- 3d coil end geometry and field optimization.
- Tolerance analysis.
- Production of drawings by means of a DXF interface.
- End-spacer design.
- Tracing of manufacturing errors.

2 Feature based geometry creation

The ROXIE program includes routines for geometrically defining coil cross-sections made of Rutherford-type superconducting cables or rectangular shaped braids. The geometric position of coil block arrangements in the cross section of the magnets is calculated from given input data such as the number of conductors per block, conductor type (specified in a cable data base), radius of the winding mandrel, and positioning and inclination angle of the blocks. The fact that the keystoning (trapezoidal shape) of the cables is not sufficient to allow their edges to be positioned on the curvature of a circle, is taken into account (c.f. Fig. 1). This effect increases with the inclination of the coil blocks versus the radial direction. The keystoning of the cable also results in a grading of the current density in the conductor as the cable is more compacted (less voids between the strands) towards the narrow side. After the geometric modelling is done, every feature (strand, cable, block, layer) can be subjected to geometric transformations such as translation, rotation, scaling, imaging, while constraints are defined for these operations in order to avoid penetration or physically meaningless structures. Not only can the geometric properties of the magnet be changed in the optimization process but so also can its material properties (in our case, for example, the number of strands, current density in conductors and strands, filling factors, unit price etc.)

3 Conceptual design using genetic algorithms.

The optimization problem associated with superconducting magnet design involves multiple, conflicting objectives, which must be considered simultaneously. The solution process for these so-called vector-optimization problems [6] is threefold, based on decision-making methods, methods for treating nonlinear constraints, and optimization algorithms for minimizing the objective function [7]. In the constraint formulation the optimization problem reads:

$$minA_{SC} \tag{1}$$

$$dB/dx > 223T/m \tag{2}$$

$$M_{ss} > 0 \tag{3}$$

$$b_6 < 0.1 \cdot 10^{-4} \tag{4}$$

$$b_{10} < 0.001 \cdot 10^{-4} \tag{5}$$

$$b_{14} < 0.0001 \cdot 10^{-4} \tag{6}$$

For the definition of the relative field errors b_6, b_{10}, etc. at a radius of 10 mm in the aperture, and for the definition of the quench-margin M_{ss} referre to the chapters below. A_{SC} is the surface of the superconducting material in the cross-section to be minimized. dB/dx is the field gradient. The number of coil blocks was limited to 4. The resulting design variables for the optimization problem are the number of turns per block, the positioning and the inclination angle of two blocks, and the current in each turn. The constrained optimization problem is transformed by an exact-penalty transformation. For the minimization of the resulting objective function, genetic algorithms are used.

In genetic algorithms, each trial solution is coded as a vector (chromosome) $\vec{X}$ with elements being described as chromosomes. Holland [8] suggests a representation of chromosomes by binary strings. As our problem is a mixture of continuous and integer, the different parameters are combined by linear sampling of the floating-point parameters and Gray-encoding of the integers into a binary string. The current in the conductors and the angles of the coil-blocks were encoded by 4 bit strings while the number of turns per block were encoded by 3 bit strings each, thus resulting in chromosomes of 32 bits. The selection operator guarantees convergence to an optimum by keeping the better chromosomes and discarding the less fit ones. Using the standard operation to retain the better half of the chromosomes reduces diversity generation by generation thus leading to gene-pools unable to profit from further crossover (recombination of bit strings of two chromosomes by swapping the strings at a random point). Therefore the diversity of the population is guaranteed by a so-called niching mechanism. After a new offspring is generated by means of crossover, the gene with the smallest hamming-distance (least difference in bits) is located and replaced if its fitness is worse than that of the offspring. Niching not only increases diversity, but provides a number of local minima for further investigations since not all the objectives (e.g. manufacturing considerations for coil winding and collaring) can be included in the objective function. A population size of 40 chromosomes has then been proved to be sufficient. The crossover probability was chosen as 0.8. The mutation operator avoids preliminary convergence of the entire population towards a local minimum. The mutation rate is 0.005. For our parameter sets of 32 bits about 3000 function evaluations were performed. Fig. 1 shows 3 different designs that result from this conceptual design phase.

Fig. 1 top shows a design that would be difficult to manufacture as the outer block has a higher angle than the inner block thus making the collaring difficult, i.e., requiring special shimming. The most efficient design in terms of gradient and conductor material is the design displayed in Fig. 1 bottom, with a conductor distribution of 8,7,8,2. In order to increase the size of the copper wedge between the two outer blocks, and in order to confirm with the base-line SACLAY design, one conductor in the first outer block was suppressed for the further studies.

4 Calculation of field errors due to persistent currents and coupling currents

Besides geometrical field errors due to the conductor placement, additional field distortions are caused by persistent currents in the superconducting filaments and coupling currents between the strands in the cable (ISCC). The persistent currents and ISCCs in each strand of each turn can be determined from the local field distribution in the coil cross-section. The resulting field errors due to these currents in all the turns of the coils can then be calculated using Biot-Savart's law.

In the outer region of a superconducting filament, subject to an applied magnetic field, currents with density J_c are generated, which screen the interior of the filament. At full penetration of the screening currents in the filament, the magnetization M (i.e. the magnetic moment per unit volume) is

$$M = -\frac{2\mu_0}{3\pi} J_c(B,T)d \tag{7}$$

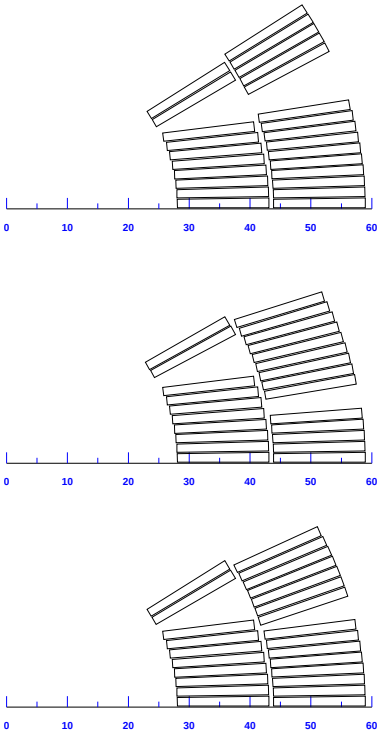

Fig. 1: Resulting coil block distributions from optimization using genetic algorithms and niching mechanism

with d the filament diameter and the critical current density J_c. Protons will be injected into the LHC at rather low field levels, where J_c and hence M are large. A typical value for M at $B = 0.5\ T$ and $T = 1.8\ K$ is about 30 mT for $d = 6\ \mu m$ [9].

Inter-strand coupling currents (ISCCs) flowing in and between the strands of the cable are generated if the cable is subject to a varying field, i.e. during ramping of the magnet. The ISCCs are proportional to:

$$I_{c,max} \approx \frac{L_p w N_s}{R_c} \frac{dB}{dt} \tag{8}$$

with L_p the twist length of the strands, w the cable width, N_s the number of strands in the cable and R_c the contact resistance between two crossing strands. Using a network model of the Rutherford type cable, in which the strands are connected through contact resistances, the coupling currents can be calculated using Kirchhoffs laws. Typical values in the strands near the edges of the cable are a few amperes for the foreseen ramp-rate for LHC (dB/dt=6 mT/s) and R_c=10 $\mu\Omega$ [10].

The resulting field errors due to these currents are given in Table 1. Both types of field errors follow the symmetry of the quadrupole field so that only the normal even harmonics b_2, b_6, b_{10}, ... are generated. Due to uncertainties in the magnetization of the filaments and in R_c over the cross-section of the coils, additional field distortions are present. In Table 2 an estimate is given of these errors assuming a 3% variation in the persistent currents and a 30% variation in R_c.

Order	Persistent curr. d=6μm, T=1.8K	Coupling curr. 0.18T/m/s, R_c=14$\mu\Omega$
b_2	-5.6	16.70
b_6	-0.54	0.020
b_{10}	0.0018	-0.0008

Table 1. The predicted errors at injection gradient (14.5 T/m) of the LHC lattice quadrupole due to the magnetic moment of the persistent currents and the inter-strand coupling currents during ramping (in units of 10^{-4} of the main field at r=10 mm).

Order	Persistent curr. d=6μm, T=1.8K $\Delta M/M$=0.03		Coupling curr. 0.18T/m/s, $R_c = 14\mu\Omega$ $\Delta R_c = 4\mu\Omega$	
n	b_n	a_n	b_n	a_n
1	1.9	1.9	1.6	1.6
2	0.75	-	2.7	0.5
3	0.32	0.32	1.	1.
4	-	0.2	0.2	0.4
5	0.04	0.04	0.05	0.05
6	0.01		0.012	0.012

Table 2. The predicted random errors in the LHC lattice quadrupole due to uncertainties in M and Rc (in units of 10^{-4} of the main field at r=10 mm).

A decrease of the field errors due to the ISCCs can be obtained by increasing R_c, which can be achieved by applying a proper coating onto the strand surface. Decreasing the filament diameter provides the only possibility to reduce M since J_c has to be as large as possible in order to obtain a compact high-field magnet. Since the lower limit of d is about 5-7 μm, important errors still remain and have to be corrected for with the coil-block geometry. The final optimization of the coil cross-section with partial compensation for the persistent current multipole errors is performed using deterministic search methods, as described in the next section.

5 Optimization of the coil cross-section

The aim of this design step is to find a coil cross-section with a part compensation of the persistent current effects by an appropriate placement of the coil blocks. As the number of ampere turns are not varied in this design phase, a relatively simple least-squares objective function

$$min(t_1(b_6 - 0.5)^2 + t_2(b_{10} + 0.001)^2 + t_3(b_{14} - 0)^2) \tag{9}$$

is minimized using the deterministic optimization algorithm EXTREM [11]. For the 4 remaining degrees of freedom (inclination and positioning angle of the two outer blocks) about 100 function evaluations have to be carried out. The weighting factors t_1 - t_3 had to be adjusted in an iterative process to t_1 = 10., t_2 = 100., t_3 = 8000. The optimized quadrupole cross-section is shown in Fig. 2.

6 Optimization of the iron cross-section

The influence of the iron magnetization is taken into account by means of a finite element calculation based on a reduced vector potential formulation. As explained in the contribution by Biro, Preis and

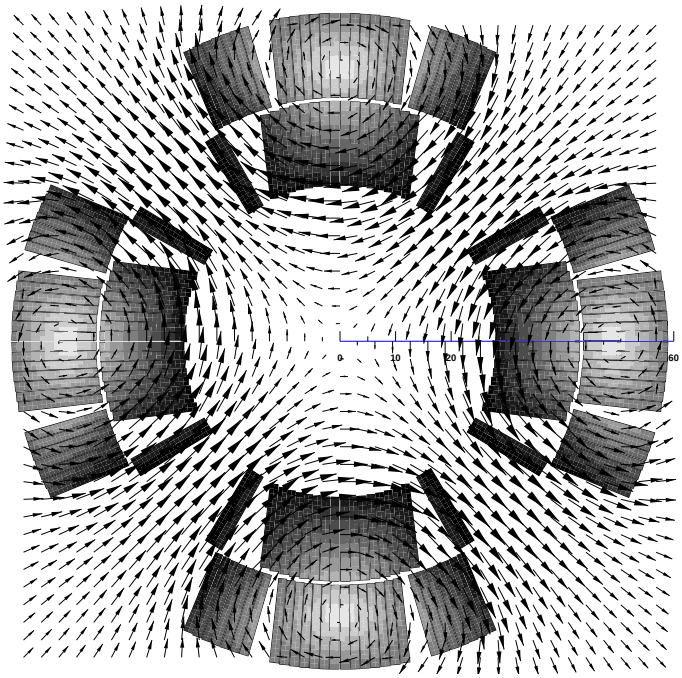

Fig. 2: Optimized quadrupole cross-section. Display of the quadrupole field and the field modulus in the coils.

Paul, this avoids the meshing of the coil, which is advantageous as the field errors are very sensitive to modelling errors of the conductor placement. The method also allows us to distinguish between the coil and the iron effects and to accurately calculate the multipole content as a function of the excitation. The peak field in the coil, which is calculated neglecting the self field of the strands, determines the margin to quench at the nominal field (see also Appendix B). As can be observed in general in quadrupole magnets, the variation of multipole errors in the aperture is relatively insensitive to the excitational current in the coils as the saturation effects are less pronounced than in the dipole magnets. The iron magnetization in the twin-aperture magnet cross-section as designed by SACLAY, a variant of that described in [4], causes the additional field errors as given in Table 3. A further minimization of these effects was not necessary. Fig. 3 shows the reduced field in the cross-section. The margin to quench is 80.3 % resulting in a gradient at quench of 277 T/m.

Order	Coil field		Coil in yoke	
	Injection	Nominal	Injection	Nominal
b_1	-	-	-10.7	-20.8
b_3	-	-	-0.37	-0.41
b_4	-	-	-0.018	-0.028
b_5	-	-	-	-
b_6	-0.07	0.47	-0.07	0.48
b_7	-	-	-	-
b_8	-	-	-	-
b_9	-	-	-	-
b_{10}	-0.0011	-0.0029	-0.0011	-0.0029

Table 3. The predicted field errors due to coil geometry and persistent current effects in the LHC lattice quadrupole at injection field level and nominal operation. The effect of the two-in-one iron yoke with saturation can be seen from the right hand columns. Note that the values given at injection field

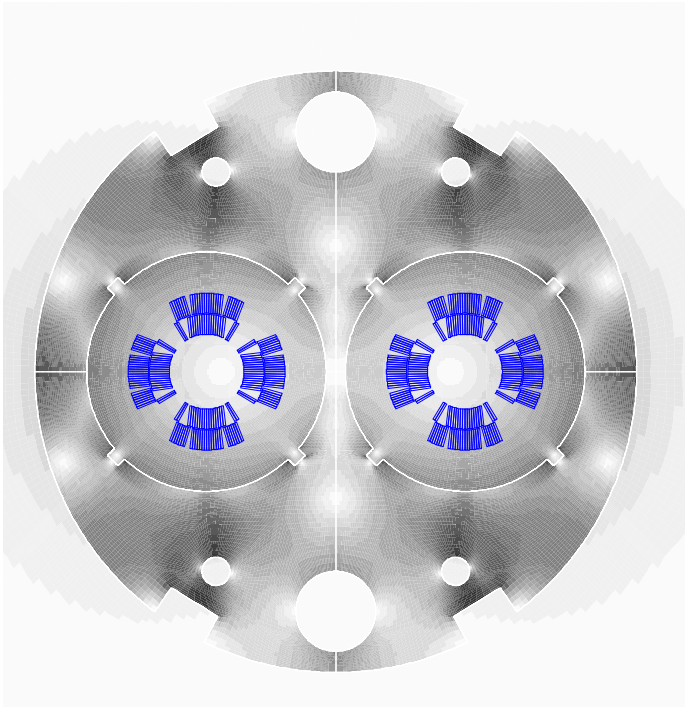

Fig. 3: Magnet cross-section with reduced field. Note that the center of the quadrupole is shifted towards the center of the yoke. The iron magnetization is therefore screening the two-in-one effect visible in the excitational field.

level contain the effects from persistent currents.

7 Quench simulation

Studying the behaviour in the event of transition to the resistive state (quench) is also an important consideration during the design phase of superconducting magnets. The aim of these studies is to know whether or not the magnet is self-protected against resistive transitions, and how to protect it in case the quenches should threaten the integrity of the magnet. A simulation package called QUABER [12] has been developed at CERN in order to investigate the behaviour of accelerator superconducting magnets in the event of a quench. This package has been built up in the environment of the commercial network analysis program SABER [13], using its associated high level design language MAST.

The network solver deals with a set of different thermo-electrical models contained in templates (simulator subprograms), which model the quench spread throughout the coils according to the different propagation mechanisms (original quench and its propagation, heater-provoked quench and its propagation, etc.). In the definition of the electrical circuit the different blocks of the magnet are represented by coupled inductances and variable quench resistances. In the calculation of both quench resistances and temperature maps, the simulator takes into account the magnetic field distribution throughout the coils. The distribution of the magnetic field as well as the mutual and self-inductances are calculated with ROXIE and interfaced into QUABER.

The basic equation that links the temperature of the conductor with the current is given by the heat balance per unit of volume under adiabatic conditions [14]:

$$\int_{t_0}^{t} i^2(t)dt = A_{Cu}A_T \int_{T_0}^{T} \frac{C(T)}{\rho_{Cu}(B,T,RRR)}dT, \tag{10}$$

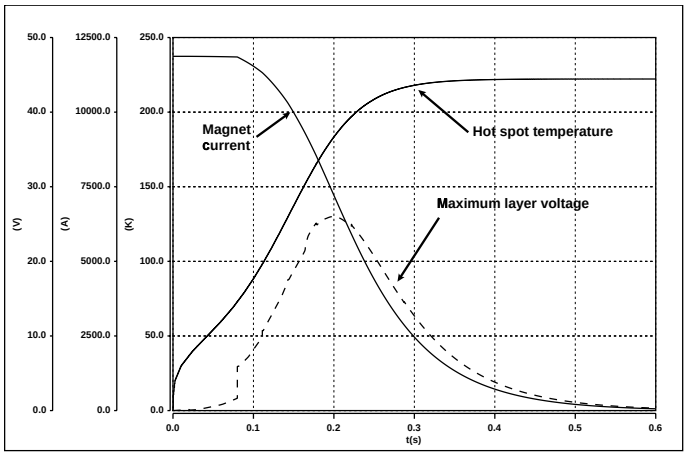

Fig. 4: Results of quench simulation

where A_{Cu} is the section of copper of a conductor, A_T the whole section of the conductor, C(T) the average specific heat of the conductor, and $\rho_{Cu}(B, T, RRR)$ is the resistivity of the copper as a function of magnetic field, temperature and the residual resistivity ratio (i.e. the ratio between copper resistivity at 300 K and at 4.2 K in absence of magnetic field). The term on the left side of the equation expressed in units of 10^6 is called MIIT and represents the quench load. The term on the right represents the quench capacity of a given superconducting cable. From this equation the map of temperature T in the coils as a function of time can be calculated.

It is assumed that a quench starts in the high field region of the outer layer at nominal current (11.8 kA) and propagates longitudinally and transversally to the neighbouring turns. The initial longitudinal quench velocity is 15 m/s and the transition propagates transversally with a turn-to-turn delay of 30 milliseconds (values according to experimental measurements). The magnet is protected by strip heaters covering the full length of 6 turns per pole in the outer layer shells. The quench heaters are effective after a delay of 80 milliseconds from the quench onset. Since the magnet is by-passed through a cold diode, the coils will dissipate the full energy stored in the magnet. The maximum temperature (hot spot) and the maximum voltage across one layer in one pole (see Fig. 4) are acceptable and qualify this magnet from the simulation point of view for the operation under the LHC machine conditions.

8 3d coil end geometry and field optimization

When designing the 3d coil geometry, the shape of the coil is determined by the objectives of maximizing the radius of curvature in the end, applying as little *hard-way* strain as possible to the cable, and optimizing the multipole content of the integrated field. The input parameters for the coil end generation are the z position of the first conductor of each coil block, its inclination angle, the straight section and the size of the inter turn spacers between the conductors. It is assumed that the upper edges of the conductors follow ellipses, super-ellipses or circles in the developed plane defined by their radial position in the straight section. A de-keystoning factor can be defined for the purposes of considering a cable-shape change in the ends caused by the winding process and the fact that a Rutherford-type cable made of strands does not have the properties of a solid beam. By shifting the relative position of the coil blocks the integrated multipole field can be optimized. For this purpose an objective weighting function is used and the algorithm EXTREM is applied. As the 3d calculations are very time consuming only 60 function evaluations are performed.

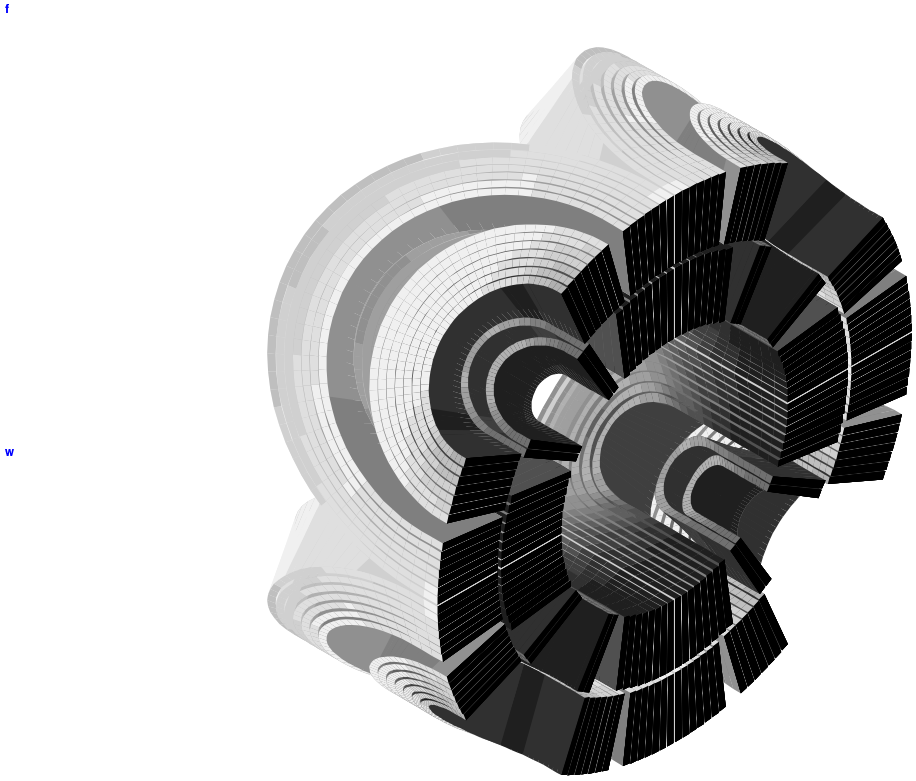

Fig. 5: Artist view of the coil end together with the electromagnetic forces parallel and perpendicular to the broad face of the cable, displayed as a gray scale.

The average field errors along the coil end from the onset of the end towards z=80 mm are for the optimized design b_6=-3.7, b_{10}=-0.066, b_{10}=-0.0035 (all in units of 10^{-4}) for an equivalent magnetic length of the end of 32 mm. As the magnet is long (3.10 m magnetic length) with respect to length of the coil end, the field errors resulting from the coil end design are acceptable. Fig. 5 shows an artist view of the coil end together with the electromagnetic forces displayed in the local conductor coordinate system, i.e., parallel and perpendicular to the broad face of the cable. Fig. 6 shows a cut through the coil end (yz plane) and the electromagnetic forces in azimuthal direction acting on the coil end. The size of the shims placed at the mid-plane before collaring the end has to be chosen such that the prestress is higher than the electromagnetic forces at full excitation.

9 Tolerance and manufacturablity analysis.

From the sensitivity matrix (which can be transferred via a CSV interface into spread-sheet programs, e.g., EXCEL) the multipole content can be evaluated as a function of the tolerances in coil block positioning, coil size, asymmetries resulting from the collaring procedure etc. This matrix is too big to be shown here, however, important conclusions can be drawn such as:

- For the coil optimization it is assumed that the shape is determined by the winding mandrel on the inner diameter of the coil. If, however, after curing and collaring the coil shape is determined by the collar on the outer diameter of the coil, the displacements would cause a b_6 of 0.37 units and a b_{10} of 0.006 units. That is virtually as large as the effect of the persistent currents!
- One coil being radially displaced by only 0.01 mm would cause b_1 and a_1 of $\pm$ 0.78 units, b_3 and a_3 of $\pm$ 0.36 units and a b_6 of 0.47 units.

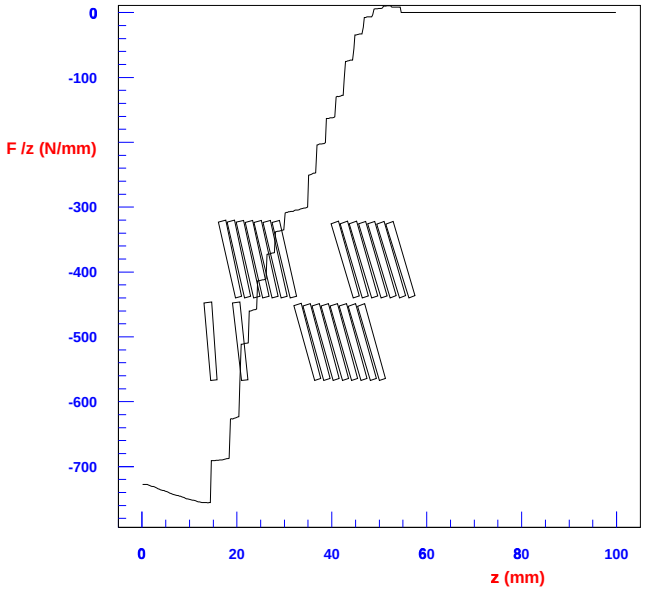

Fig. 6: Electromagnetic forces in azimuthal direction at nominal field acting on the coil end. The size of the shims placed at the mid-plane before collaring the end has to be chosen such that the prestress is higher than the electromagnetic forces at full excitation.

These two examples show how important it is to control the coil positioning during the assembly process of the magnet.

10 Production of drawings by means of the DXF interface.

The DXF interface creates files for the drawing of the cross-section in the xy and yz planes of the magnet, the developed view and the polygons for the end-spacer manufacture thus eliminating draughting work of about 2 man-days.

11 End-spacer design and data transfer for the CNC machining

The shape of the end-spacers is determined by the shape and position of the coil blocks as found in the field optimization process. The surfaces to be machined are described by 9 polygons, which are transferred into a CAM system, e.g., CATIA, for the calculation and emulation of the cutter movements for machining the piece. As an interface an ASCII file, a VDA file and a DXF file is available. The spacers are machined by means of a 5-axis CNC machine from glass-epoxy tubes (G11). Because of the abrasive nature of the glass dust, diamond tools must be used. Fig. 7 shows an artists view of the endspacers (outer layer coil) for the quadrupole.

12 Inverse field calculation for the tracing of manufacturing errors.

The dimensions of the active parts of the coils are impossible to verify under their operational conditions after their deformation due to manufacture, warm pre-stressing, cool-down and excitation. The inverse problem solving consists of using optimization routines to find distorted coil geometries which exactly produce the multipole content measured [16]. The function to be minimized in the inverse field

Fig. 7: Artists view of the endspacers for the quadrupole, outer layer coil

computation problem yields

$$min \sum_{i=1}^{10} p_i \cdot (b_i^*(\vec{X}) - b_i)^2 + q_i \cdot (a_i^*(\vec{X}) - a_i)^2 \tag{11}$$

where $b_i^*(\vec{X})$, $a_i^*(\vec{X})$ are the calculated and b_i, a_i are the measured multipoles. $\vec{X}$ is the vector of the design variables for the inverse problem. The p_i and q_i are weighing factors that compensate for the different numerical values of the residuals. Because of the non-symmetric nature of the geometrical coil positioning errors, a large number of design variables result for the inverse field problem. It is therefore assumed that the positioning errors hold for an entire coil block rather than for individual conductors. The design variables are the possible perturbations, in radial direction, of all 24 coil-blocks plus 16 azimuthal displacements of the blocks. It is assumed that the blocks that are connected at the mid-plane are free to move only by the same amount. Because of the fact that there are far more degrees of freedom than objectives the problem is ill-posed. Therefore a *regularization* term is added to Eq. (11)

$$\sum_{i=1}^{30} q_i \cdot (x_i - 0)^2 \tag{12}$$

to make sure that the coil-block displacements stay as small as possible. As a minimization algorithm the Levenberg-Marquard method is applied.

Table 4 gives the measured multipole distribution [15] in the straight part of a previously built quadrupole magnet with slightly different conductor distribution [2] together with the expected (intrinsic) values.

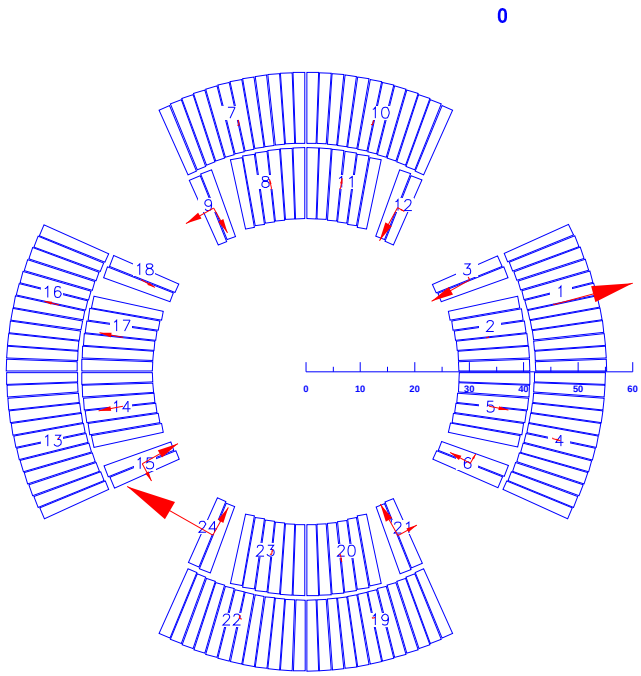

Fig. 8: Coil-block displacement of a quadrupole prototype, biggest vector represents a 0.25 mm displacement

	Measured		Intrinsic	
n	Normal	Skew	Normal	Skew
1	-	-	-	-
3	0.27	0.36	-	-
4	0.01	-0.21	-	-
5	-0.03	0.	-	-
6	-0.23	-0.02	0.107	-
7	0.01	0.	-	-
8	0.	0.	-	-
9	0.	0.	-	-
10	-0.01	0.	-0.0087	-

Table 4: Measured multipoles in the straight part of one aperture and intrinsic values as expected from the coil design, units of 10^{-4} at 10 mm, current 10000 A

The result of the inverse problem computation can be seen in Fig. 8. The arrow length of the most important displacement corresponds to 0.25 mm in block no. 24. All other displacement arrows are to scale. These results also allow to check the need for a mandrel inside the coil aperture in the final collaring phase (in fact, the coil assembly mandrel was extracted before the final compression of the collars). The displacements in Fig. 8 show some inward movement of the small coil blocks which possibly could have been avoided.

REFERENCES

[1] CERN, European Organisation for Nuclear Research.: The Large Hadron Collider, Conceptual Design, CERN/AC/95-05

[2] Baze, J.M., Cacaut, D., Chapman, M., Jacquemin, J.P., Lyraud, C., Michez, C., Pabot, C., Perot, J., Rifflet, J.M., Toussaint, J.C., Vedrine, P., Perin, R., Siegel, N., Tortschanoff, T.: Design and fabri-

cation of the prototype superconducting quadrupole for the CERN LHC project, 12th International conference on magnet technology, Leningrad, USSR, 1991

[3] Henrichsen, K., Rodriguez-Mateos, F., Siegel, N., Tortschanoff, T, Rifflet, J.M., Cortella, J., Deregel, J., Genevey, P., Perot, P., Vedrine, P.: Cryogenic and mechanical measurements of the first two LHC lattice quadrupole prototypes, EPAC 94, London, 1994

[4] Tortschanoff, T., Parma, V., Rohmig, P., Peyrot, M., Rifflet, J.M., Vedrine, P., Vincent, D.: The short straight section for the LHC, to be published at the Particle Accelerator Conf., 1997.

[5] Karppinen, M., Russenschuck, S., Ijspeert, A.: Automated Design of a Correction Dipole Magnet for LHC, EPAC 1996

[6] Cohon, J.L.: Multiobjective Programming and Planning. Academic Press, New York, 1978

[7] Russenschuck, S.: Synthesis, inverse problems and optimization in computational electromagnetics, International Journal of numerical modelling: Electronic networks, devices and fields, Vol. 9, John Wiley & Sons, 1996

[8] Holland, J.H.: Adaption in Natural and Artificial Systems (An Introductory Analysis with Applications to Biology, Control, and Artificial Intelligence) The MIT Press, Cambridge, 1995

[9] Wolf, R.: Persistent currents in LHC magnets, LHC Note 158, September, 1991.

[10] Verweij, A. P., Wolf, R.: Field Errors due to Interstrand Coupling Currents in the LHC Dipole and Quadrupole, CERN/AT-MA internal note 94-97, March, 1994.

[11] Jacob, H.: Rechnergestuetzte Optimierung statischer und dynamischer Systeme, Springer 1982

[12] Hagedorn D., Rodriguez-Mateos, F. ”Modelling of the quenching process in complex superconducting magnet systems,” IEEE Trans. Magn., vol. 28, pp. 366-369, January 1992.

[13] SABER is a trademark of Analogy, Inc.

[14] Wilson, M. N.: Superconducting Magnets, Oxford: Clarendon Press, 1983, pp. 200-208.

[15] Devred, A.: private communication

[16] Russenschuck, S., Tortschanoff, T., Ijspeert, A., Siegel, N., Perin, R.: Tracing back measured magnetic field imperfections in LHC magnets by means of the inverse problem approach,IEEE Transactions on Magnetics, Vol-Mag 30, 1994

[17] Preis, K., Bardi, I., Biro, O., Magele, C., Renhart, W, Richter, K.R., Vrisk, G.: Numerical analysis of 3d magnetostatic fields, IEEE Transactions on Magnetics, 27, 3798-3803, 1991